

THIRD EUROPEAN ROTORCRAFT AND POWERED LIFT AIRCRAFT FORUM

Paper No 26

A MODAL APPROACH
TO
GROUND RESONANCE

K.H. GRIFFIN

COLLEGE OF AERONAUTICS, UNITED KINGDOM

September 7-9, 1977

AIX-EN-PROVENCE, FRANCE

ASSOCIATION AERONAUTIQUE ET ASTRONAUTIQUE DE FRANCE

ERRATA

p.4 Eqn.(6) should read:

$$\begin{aligned} z_f &= Z_1 e^{i\omega_{f_1} t} + Z_2 e^{i\omega_{f_2} t} + Z_3 e^{i\omega_{f_3}(1-i\alpha)t} + Z_4 e^{i\omega_{f_3}(1+i\alpha)t} \\ z_g &= \zeta_1 Z_1 e^{i\omega_{f_1} t} + \zeta_2 Z_2 e^{i\omega_{f_2} t} + \zeta_3 Z_3 e^{i\omega_{f_3}(1-i\alpha)t} + \bar{\zeta}_3 Z_4 e^{i\omega_{f_3}(1+i\alpha)t} \end{aligned} \quad (6)$$

p.5 4th line after eqn.(8): for "experimental" read "exponential" .

Fig.8 The legend should read " $\Lambda_1 = 0.05, \Lambda_2 = 0, \Lambda_3 = 0.05$ "

Fig.13 The three sets of curves are for $\lambda_f = 0, 0.05, 0.20$ respectively.

A MODAL APPROACH TO GROUND RESONANCE

K.H. Griffin, College of Aeronautics, Cranfield, U.K.

1. Introduction

Nearly forty years ago Coleman, in Ref. 1, derived the basic equations for the elementary treatment of ground resonance by considering the motion in its own plane of a rotor with rigid blades hinged at their roots as illustrated in Fig.1. Many other workers have built on this contribution.

For the n -bladed rotor ($n > 3$) there is one equation of motion corresponding to each blade and three overall equations for the helicopter as a whole (fore/aft, lateral and rotational). Coleman transformed the blade equations into two linear and one rotational one together with $(n-3)$ equations involving combinations of blade motion which have neither linear nor angular momentum. These $(n-3)$ equations and the two angular equations all involve stable motions, although it is through non-linear terms in the angular momentum equations that the work done to drive the ground resonance oscillations is transmitted. Only the four linear momentum equations control the ground resonance motion directly and it is with these equations that most work on the subject has been concerned. They contain two important parameters: λ_g and λ_f depending respectively on blade root and undercarriage damping. Coleman derived his equations in complex variable form and the condition for entering and leaving the self-excited range was the vanishing of the determinant of the coefficients of these equations. The real part led to an equation in $\lambda_f \lambda_g$ - the "damping product" - and the imaginary part to one in λ_f / λ_g .

In a recent paper (Ref.2) Price makes a slight but significant modification to the determinant which has the effect of presenting two alternative equations, one of which involves λ_f (undercarriage damping) only. This enables Price to draw conclusions, particularly about λ_f , in a more convenient and accessible form than in the original work. The present paper returns to the original Coleman equations and considers their physical significance expressed in the relationships between hub and blade motion.

2. Basic Equations of Motion

Coleman uses the complex variable $z_f = x_f + iy_f$ to describe the displacement of the hub in the rotorplane from its position of static equilibrium. He transforms the rotorblade displacement angles β_k into a series of complex variables ζ_j of which only ζ_1 appears in the linear momentum equations. Coleman's ζ_1 in fact represents the displacement from the rotor hub centre of the centre of mass of the blade system. In this paper it will be called $z_g = x_g + iy_g$; z_f and z_g are illustrated in Fig.2. Coleman's equations for the relation between the blade and hub motion may be written as

$$\ddot{z}_g - 2i\omega\dot{z}_g - \omega^2 z_g + \lambda_\beta (\dot{z}_g - i\omega z_g) + (\Lambda_1 \omega^2 + \Lambda_2) z_g + \ddot{z}_f / 2(1+r^2/b^2) = 0 \quad (1)$$

where ω is the rotor angular velocity, $\Lambda_1 = ab/(b^2+r^2)$ and is a non-dimensional parameter representing the blade hinge radius, whilst $\Lambda_2 = K_\beta/m_b(b^2+r^2)$ and $\lambda_\beta = B_\beta/m_b(b^2+r^2)$ respectively give the non-dimensional blade-root spring stiffness and damping constant. Equation (1) may be thought of as governing the blade response to any imposed hub motion. The overall equations of motion are

$$2(1+r^2/b^2)\Lambda_3 \ddot{z}_g + \ddot{z}_f + \lambda_f \dot{z}_f + \omega_r^2 z_f + (\Delta m \ddot{z}_f + \Delta \lambda \dot{z}_f + \Delta \omega_r^2 z_f) = 0 \quad (2)$$

The coefficients of Z and its derivatives arise from the differences in fuselage inertia, damping and stiffness properties between the x and y directions and will be ignored for the moment, as in the greater part of the present discussion the fuselage will be assumed to give isotropic support to the rotor. m_f, B_f, K_f are the mean (between x and y properties) inertia, damping and stiffness constants for the fuselage. $M = m_f + nm_b$, where m_b is the mass of a single blade, $\Lambda_3 = nm_b b^2/2M(b^2+r^2)$, $\omega_r^2 = K_f/M$, $\lambda_f = B_f/M$

3. Modes of Motion

Equations (1) and (2) are linear differential equations in z_f and z_g with constant coefficients. The only possible solution is of the form $z \propto \exp(kt)$ where k may be complex. It is convenient to modify the notation and work in terms of $\exp(i\omega_f t)$ where ω_f may be complex, but for much of the motion is real. In this case the solution is a circular whirl, while ω_f complex gives an equiangular spiral. Equations (1) and (2) can then each be regarded as giving an expression for the ratio of z_g to z_f . One may write $\zeta = 2(b^2+r^2)z_g/b^2z_f$ when (1) and (2) become respectively

$$\zeta = F(\omega_f, \omega) = -\omega_f^2 / \left[(\omega_f - \omega)^2 - i\lambda_\beta(\omega_f - \omega) - (\Lambda_1\omega^2 + \Lambda_2) \right] \quad (3)$$

$$\zeta = G(\omega_f) = \left[(\omega_r/\omega_f)^2 - 1 + i\lambda_f(\omega_r/\omega_f) \right] / \Lambda_3 \quad (4)$$

The parameter ζ describes the mode of the motion, namely the relationship between z_g and z_f as shown in Fig.2. Equation (3) is quite general and displays the relation between blade and hub motion for any circular or spiral whirl. Equation (4) shows whether or not such a motion can be supported by the undercarriage forces.

It is easiest to see the inter-relation between the two conditions in the undamped case $\lambda_\beta = \lambda_f = 0$. Here for ω_f real (circular whirling) F and G are both real and so the hub and the blade system mass centre move round concentric circles sharing a common radius. In Fig.3, plotted for a particular value of ω , the solid curve is that for F and the dotted curve that for G . The points A, A' where $G = 0$ are for $\omega_f = \pm\omega_r$, the natural frequencies where the blade and hub oscillate in unison on the undercarriage. At high positive and negative whirl velocities $\zeta \rightarrow -1/\Lambda_3$ and the mode is controlled entirely by balance of inertia forces; the large values of G when ω_f is small indicate that the blade inertia forces are low and are balanced by very small fuselage motions and resulting spring forces. The solid curve for F with value -1 at high whirl velocities shows that in that state the blade system mass centre stays still because any movement would generate inertia forces too large for the blade restoring forces to balance. The zero for F at $\omega_f = 0$ shows that at low whirl velocities the rotor system behaves "solidly"; while the two vertical asymptotes correspond to the natural frequencies of the blades on their hinges, modified by centrifugal action and compounded with the overall rotor rotation.

4. Solutions for Whirling Motion

Fig.4 shows how F changes with rotor speed for a case where $\Lambda_2 \neq 0$. When $\omega = 0$ (Fig.4(a)) there are four points where F and G intersect, that is where a mode of feasible motion exists satisfying both equations of motion. These occur at two pairs of equal and opposite values of ω_f , corresponding to whirls in opposite directions: one pair (of lower velocity) gives positive ζ (i.e. blade system mass centre rotating with larger radius than hub) while the higher velocity pair give $\zeta < 0$, $|\zeta| > 1$ and so the blade CM rotates with small radius on the opposite side of the centre of whirl from the hub. Figures 4(b) to 4(h) follow the effect of increasing rotor velocity ω and show that there are always two motions for which ζ is negative. One of these corresponds to negative ω_f (whirling in the opposite direction to rotor rotation) and this is the only such motion: as ω increases $|\zeta|$ for this mode reduces to values less than unity.

The other motion, always that for the highest value of ω_f , has $\zeta < -1$.

It is the other two intersections which provide the interest in the motion and they are controlled largely by the vertical asymptotes of F , the natural frequencies of the blades in their rotating system. As ω increases from zero, the whirl in the same direction as ω increases its velocity and decreases $\zeta (\propto z_g/z_f)$ while the "opposite sense" whirl slows down and ζ increases to large values (i.e. small hub motion). Fig.4(c) shows the case where the whirl is just changing direction. The value of ζ at $\omega_f = 0$ appears to be 'lost' but is in fact infinite ($z_f = 0$). This corresponds to the rotor velocity ω at which Coleman notes that a constant lateral force can excite blade motions. Fig.4(d) shows the situation where both these velocities are getting closer together and in 4(e) they coalesce. This is the beginning of the self-excited range, for as 4(f) shows for higher values of ω these two motions have 'disappeared'. The disappearance, of course, is only apparent and the solutions exist with conjugate complex values of ω_f , one being an in-going (stable) spiral and the other the out-going spiral which causes ground resonance. Figs. 4(g) and 4(h) show the reappearance of the "lost" motions above the self-excited range of rotor velocity. It will be noted that in this high velocity range all motions have negative ζ . A considerable simplification of the equations occurs when $\Lambda_2 = 0$. F then becomes purely a function of (ω_f/ω) and the effect of increasing ω is to spread out the horizontal scale of the curve for F in Figs. 3 and 4.

5. Self-excited Motion

Up till now we have considered only the circular whirling motion (ω_{freal}). In order to complete the solution over the whole range of ω we must look at complex values of ω_f . It is convenient to replace ω_f by $\omega_f(1-i\alpha)$. This implies components of velocity as in Fig.5 giving a spiral angle ($\tan^{-1}\alpha$) and still an angular velocity ω_f about the spiral centre. For a given value of α the real and imaginary parts of ζ can be plotted against ω_f as shown in the perspective sketch Fig.6. Fig.6 is plainly of little value compared with Fig.4 so far as understanding the phenomena are concerned, but if the space curves of $F(\omega_f)$ and $G(\omega_f)$ are projected on to the (ζ_R, ζ_I) plane diagrams like Fig.7 result. It must be remembered that though Fig. 7 shows two apparent intersections between F and G they will in general occur for different values of ω_f and therefore are not intersections in the full three-dimensional relationship (Fig.6). However if $\Lambda_2 = 0$ (no blade root stiffness) F is a function of (ω_f/ω) and therefore merely by choosing ω (a different value for each of points A and B of Fig.7) each of A and B can be made into true intersections of F and G and provide true solutions for the motion. Similarly when $\Lambda_2 \neq 0$ variation of ω will produce different but similarly shaped curves F , and intersections can still be found.

Thus Fig.7 shows that for a given value of α (approximately the spiral angle) there are two values of ω for which such a spiral motion is possible. When α is small (nearly circular whirling) the two lobes of F are of very large radius and G is inclined at a small angle to the ζ_R axis. As α increases the lobes of F reduce in size and the slope of G increases, as illustrated in Fig.8. If α is reversed in sign both F and G are reflected in the ζ axis and so the values of ω_f and ω at which intersections occur are the same. Thus to every out-going whirling motion there corresponds an ingoing whirl, both motions having conjugate values of ζ as in Fig.9. Fig.8 shows that there is only a limited range of values of α for which solutions are possible and the sequence of crosses illustrates the variation of the mode shape parameter ζ through the self excited range, starting from A and proceeding through B (at the value of rotor velocity for which exponential spiral growth is most rapid) to the end of the self-excited range at C.

With Figs. 4 and 8 we are able to trace the development through all values of ω of the four whirling motions in terms of their mode parameters (ζ) angular velocities (ω_f) and their spiral angles ($\tan^{-1}\alpha$). In Fig.10 the history of ζ against ω is plotted. It will be seen that the pair of modes which couple together may be described as taking the opportunity of moving out

of the real plane in order to change the sign of their real part. If ζ remained wholly real it would have had to pass through the value zero, implying zero blade mass centre motion while the hub moved - an unlikely situation.

6. Considerations of Stability

Now it must be stated at this point that apart from introducing the mode parameter ζ none of the argument so far has produced any further information than is contained in Ref. 1. However it is possible to follow the complete motion by combining together at any value of ω the four solutions (ζ_1, ω_{f_1}) , (ζ_2, ω_{f_2}) , (ζ_3, ω_{f_3}) & (ζ_4, ω_{f_4}) . Thus outside the self excited range

$$\left. \begin{aligned} z_f &= Z_1 e^{i\omega_{f_1} t} + Z_2 e^{i\omega_{f_2} t} + Z_3 e^{i\omega_{f_3} t} + Z_4 e^{i\omega_{f_4} t} \\ z_g &= \zeta_1 Z_1 e^{i\omega_{f_1} t} + \zeta_2 Z_2 e^{i\omega_{f_2} t} + \zeta_3 Z_3 e^{i\omega_{f_3} t} + \zeta_4 Z_4 e^{i\omega_{f_4} t} \end{aligned} \right\} \quad (5)$$

and in that range

$$\left. \begin{aligned} z_f &= Z_1 e^{i\omega_{f_1} t} + Z_2 e^{i\omega_{f_2} t} + Z_3 e^{i\omega_{f_3}(1-i\alpha)t} + Z_4 e^{i\omega_{f_3}(1+i\alpha)t} \\ z_g &= \zeta_1 Z_1 e^{i\omega_{f_1} t} + \zeta_2 Z_2 e^{i\omega_{f_2} t} + \zeta_3 Z_3 e^{i\omega_{f_3}(1-i\alpha)t} + \zeta_4 Z_4 e^{i\omega_{f_3}(1+i\alpha)t} \end{aligned} \right\} \quad (6)$$

If one considered the motion resulting from the initial state of the hub at rest but displaced slightly, i.e.

$$z_f = Z_0, \text{ say; } \dot{z}_f = z_g = \dot{z}_g = 0 \quad (7)$$

then that motion may be calculated and examined. It is clear from Fig.4 that away from the self-excited range the values of $\zeta_1 \dots \zeta_4$ and $\omega_{f_1} \dots \omega_{f_4}$ are well separated, and so the equations for $Z_1 \dots Z_4$ found by substituting from (5) in (7) will be well conditioned, and the values of $Z_1 \dots Z_4$ will be of similar magnitude to Z_0 . The motion of the system after release will be a not necessarily simple combination of four circular whirls of different angular velocities, and a typical such result is shown in Fig.11(a). In the self-excited range, one of the basic components of the motion will be an outgoing spiral whirl and will obviously lead to motion of the type shown in Fig.11(b). A point to be noted though, is that when the self-excited range is being approached but the response is still nominally stable (Fig.4(d)) there are two component motions with similar value of ζ_i and very similar values of ω_{f_i} . This means that the columns of coefficients of the corresponding Z_i in the equations for $Z_1 \dots Z_4$ will also be similar. Thus the equations will be ill-conditioned and the two values of Z_i will be large and of opposite sign. These two motions will "beat" together and give rise to response of the form shown in Fig.11(c). If the magnification of an initial disturbance is sufficient then this is likely to be as destructive as the motion in the formal self-excited range.

7. Motion with Damping

The full expression for F and G (with ω_f where necessary replaced by $\omega_f(1+i\alpha)$) may be evaluated for given values of the parameters $\Lambda_1, \Lambda_2, \Lambda_3$ for different values of the damping parameters λ_B and λ_f and of the spiral angle parameter α . It may be noted that this approach completely separates the effect of the two damping constants. Fig.12 shows the effect of λ_B and α on F while correspondingly Fig.13 shows the effect of λ_f and α on G. It will be

seen that the general effect of damping on F and G is similar to that of α in the undamped case. Thus increasing λ_B tends to shrink the lobes of the curves for F and λ_f tends to spread the curves for G. It follows that both the damping parameters contribute towards making impossible the existence of an outgoing spiral solution. It is clearly possible, if tedious, to use such a pair of plots to predict the complete response of the system in terms of the four sets of values of ω_f , ζ and α at every value of ω . However as is usual in such self-excited systems it is simpler to find the boundaries of the self-excited range by extracting the solutions with $\alpha = 0$ which form the boundary between damped and unstable motion. The proviso at the end of the previous section about the region just outside the self-excited range should be noted here, though.

Fig.14 shows the results of such a plot for the case $\Lambda_1 = 0.04$, $\Lambda_2 = 0$, $\Lambda_3 = 0.02$, $\lambda_B = \Lambda_B \omega$. The reason for working with Λ_B rather than λ_B is that when $\Lambda_2 = 0$ the function F remains in terms only of (ω_f/ω) rather than of ω_f and ω as independent variables. Thus for a given value of λ_f the values of ω at the boundaries of the self-excited range may be plotted against Λ_B . It is then simple to transfer pairs of values of Λ_B and ω to the equivalent values of λ_B and ω . Both plots are shown in Fig.15. It is then possible, as many others have done, to plot λ_f and λ_B for stability as in Fig.16. However such a plot gives no new information and does not justify a new approach. It is much more convenient matter to look at Fig.14 to see whether or not a particular combination of λ_f and Λ_B will prevent ground resonance. It is easy to produce sets of curves of F against Λ_B for different values of Λ_1 , and transparent overlays of G against λ_f for different values of Λ_3 . These may then be rapidly compared to see whether or not self-excited oscillation is possible. The effect of Λ_2 may be allowed for by using $\Lambda_1' = \Lambda_1 + \Lambda_2/\omega^2$ iterating on values of Λ_1' once the value of ω at the centre of the self-excited range has been initially located.

8. Support Conditions Other than Isotropic

The convenience of the isotropic support condition so far considered is that it gives equation (2) polar symmetry, a property always possessed by (1). Naturally when this symmetry is lost from (2) the resulting analysis must lose some of its simplicity. If the asymmetric terms in (2) deriving from Δm etc. are included then the motion may no longer be defined in terms simply of circular and spiral whirls. It is possible to write

$$z_f = e^{i\omega_f(1-i\alpha)t} + \gamma e^{-i\omega_f(1+i\alpha)t} \quad (8)$$

where γ is a constant. Such a motion may be most clearly described when $\alpha = 0$, when it is an elliptical whirl. If γ is real then the axes of the ellipse are parallel to Ox and Oy, while complex values of γ give an ellipse inclined to those axes. The effect of α is to impose an exponential growth or decay on the elliptical motion. It follows from (3) that corresponding to expression (8) for z_f will be blade motion defined by

$$2(1+r^2/b^2)z_g = F(\omega_f, \alpha) e^{i\omega_f(1-i\alpha)t} + \gamma F(-\omega_f, -\alpha) e^{-i\omega_f(1+i\alpha)t} \quad (9)$$

It is now possible to define functions $G_x(\omega_f)$, $G_y(\omega_f)$ as in (4) but using the appropriate x- and y- properties. Furthermore if the following definitions are made:

$$F^+ = [F(\omega_f, \alpha, \omega) + \bar{F}(-\omega_f, -\alpha, \omega)] / 2, \quad F^- = [F(\omega_f, \alpha, \omega) - \bar{F}(\omega_f, -\alpha, \omega)] / 2 \quad (10)$$

the condition corresponding to $F = G$ in the isotropic case becomes

$$(F^+ - G_x)(F^+ - G_y) = (F^-)^2 \quad (11)$$

For the case of unidirectional support ($y_f = 0$) this becomes $F^+ = G_x$ and shows great similarity with the isotropic case. As it stands equation (11) does not show the separation between rotor and fuselage properties achieved until now. However it may be noted that the values of F in the range $\omega_f < 0$ are always much smaller than those for positive ω_f . If then $F(-\omega_f, -\alpha, \omega)$ is neglected compared with $F(\omega_f, \alpha, \omega)$ equation (11) reduces to

$$F = 2G_x G_y / (G_x + G_y) \quad (12)$$

If the undercarriage has similar damping ratios in the two directions then the right hand side of (12) does not differ greatly from G , and damping combinations to close the self-excited range are little different from those of the isotropic case. Figures 17 and 18 show F^+ plotted for the cases corresponding to Figures 3 and 7 respectively.

9. Conclusions

The phenomenon of helicopter ground resonance has been examined by looking separately at the equations linking the rotor motion to that of the hub and at those governing the overall vehicle motion. The conditions imposed by the first set of equations, the consequences of which are expressed here by function F , show two frequency bands with rotor motion large compared with that of the hub, at angular frequency ranges one below and one above the rotor angular velocity. These two frequency bands correspond effectively to the natural frequencies of the blades as modified by the centrifugal and Coriolis forces. It is the motion in the lower of these frequency bands only which is able to give combinations of rotor and fuselage inertia force which can be balanced by the undercarriage reactions.

The procedure of keeping separate the internal and overall equations of motion has the advantage of showing separately the effects of rotor and undercarriage damping and their relative effectiveness in any condition. The procedure may be directly extended to the case of the rigid-rooted flexible-bladed rotor by deriving the equivalent of equation (1) replacing the blade angles β_k by normal coordinates of the blades taken with their corresponding natural modes. A different function F results but with similar characteristics. For more realistic representation of the fuselage motion general equations corresponding to (2), but involving all the other fuselage displacements, may be written and solved in terms of Z_f and Z_g to give response conditions corresponding to G . These may again be compared with F , which needs no attention.

Finally, one may return to Figure 4 which shows the development of response in the simple undamped isotropic case. Ground resonance may be seen as the inability of the helicopter, in a limited frequency band, to match its rotor and overall characteristics without recourse, as it were, to spiral motion.

10. References

1. R.P. Coleman and A.M. Feingold, Theory of self-excited mechanical oscillations of helicopter rotors with hinged blades, NACA R 1351, 1958
2. H.L. Price, A single parameter technique for helicopter ground resonance studies, Symposium on Helicopter Vibrations, RAeS, London, Nov. 1976

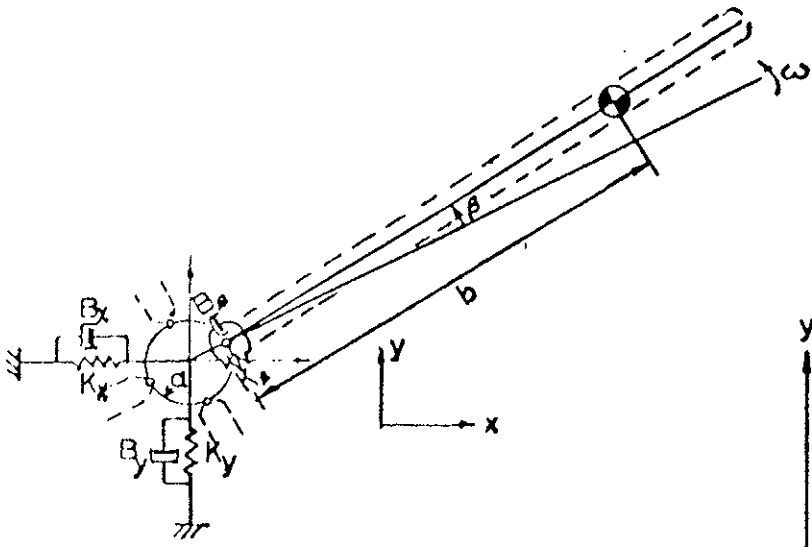


Fig. 1

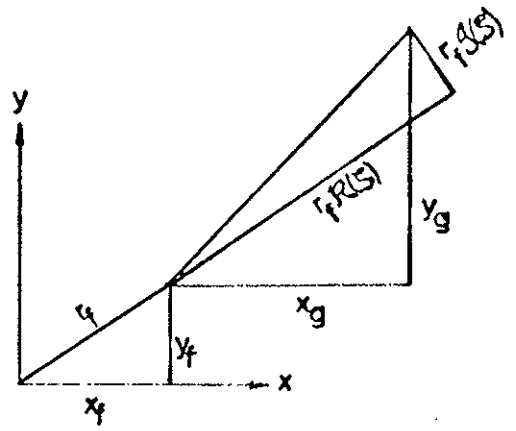


Fig. 2

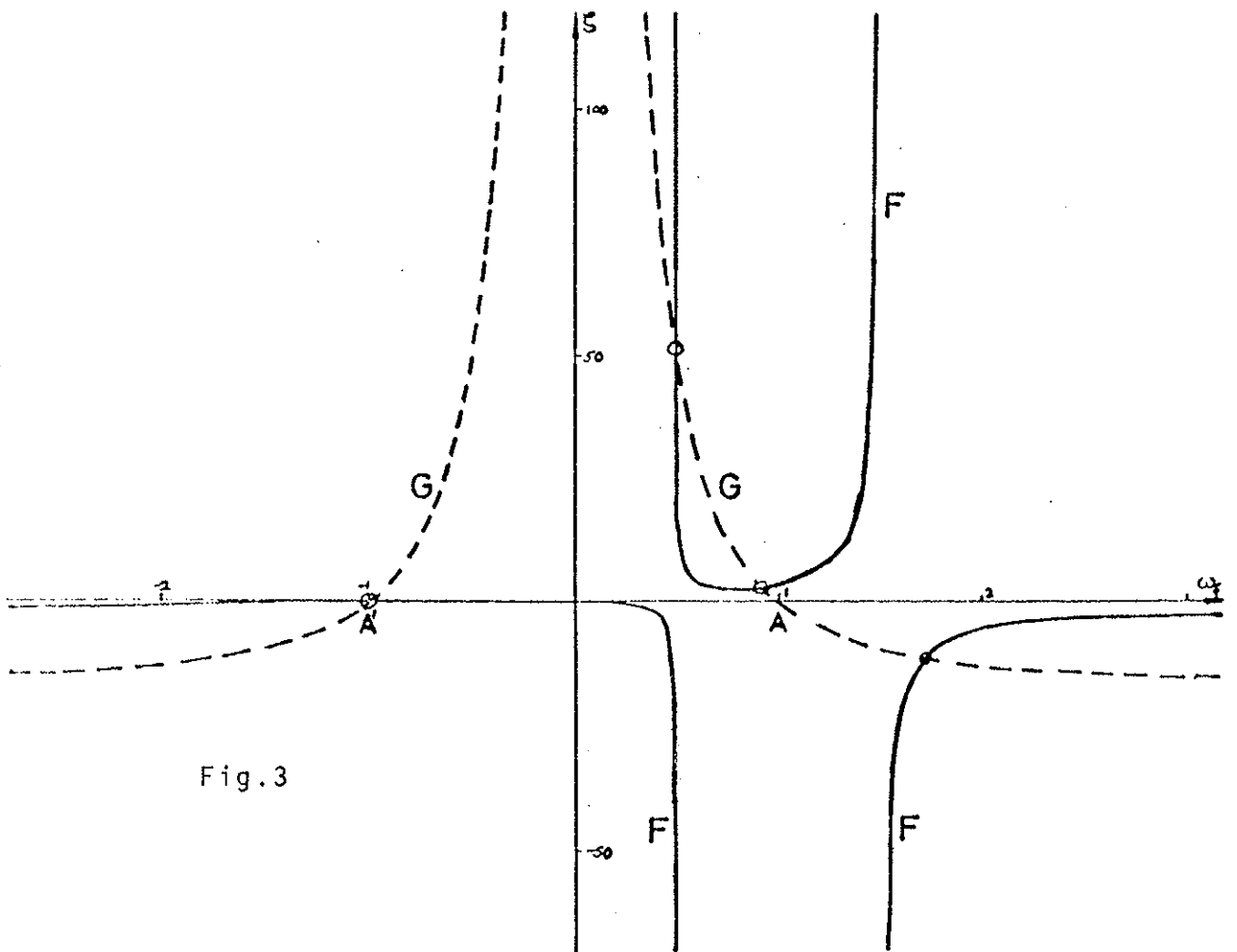
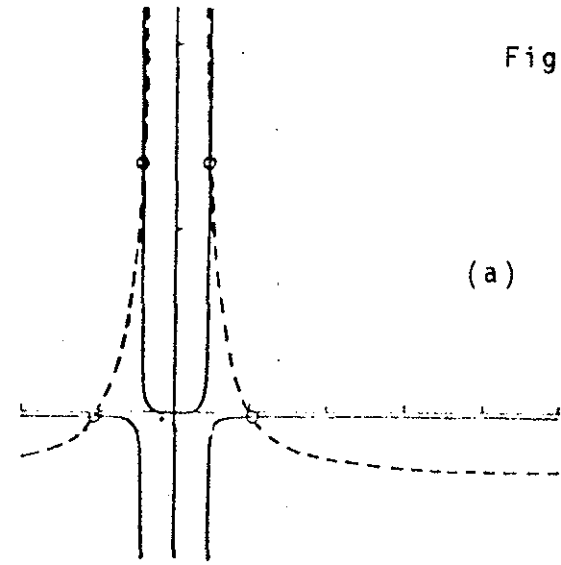
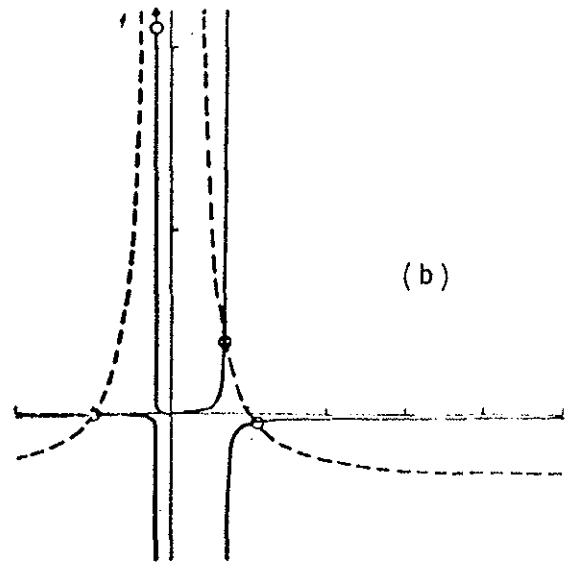


Fig. 3

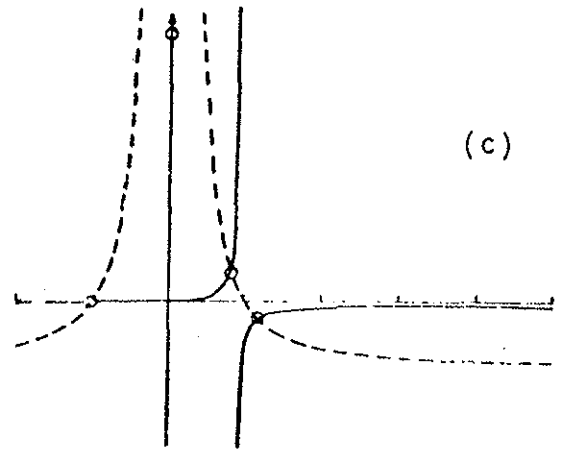
Figure 4



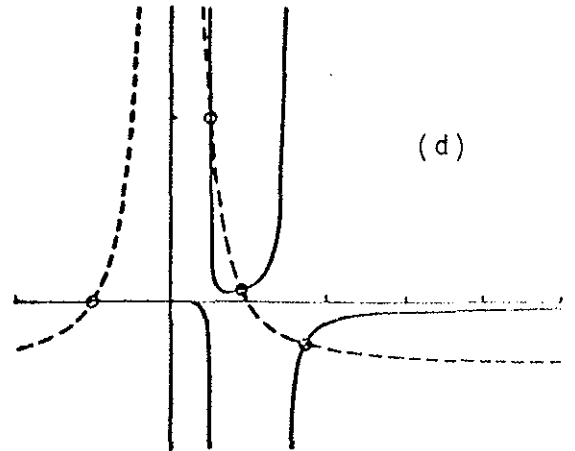
(a)



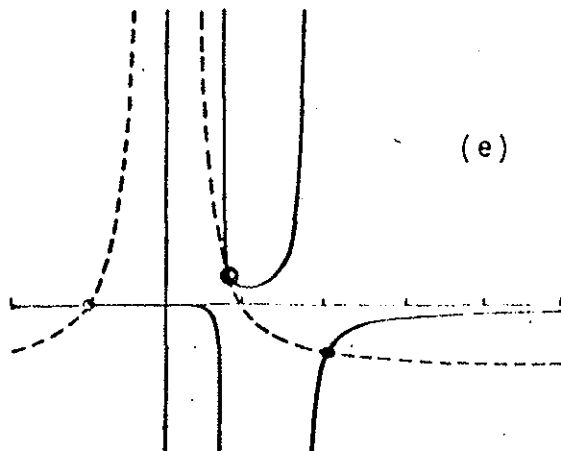
(b)



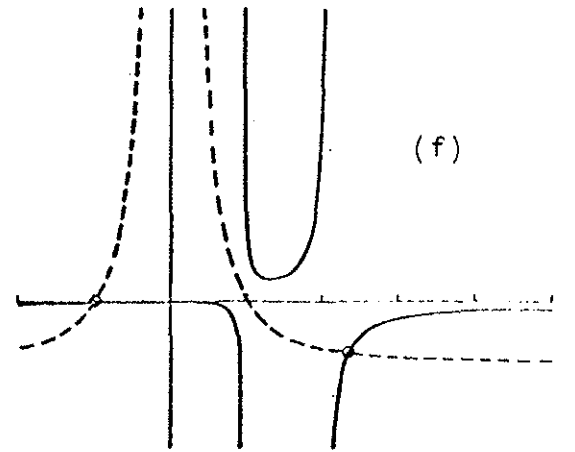
(c)



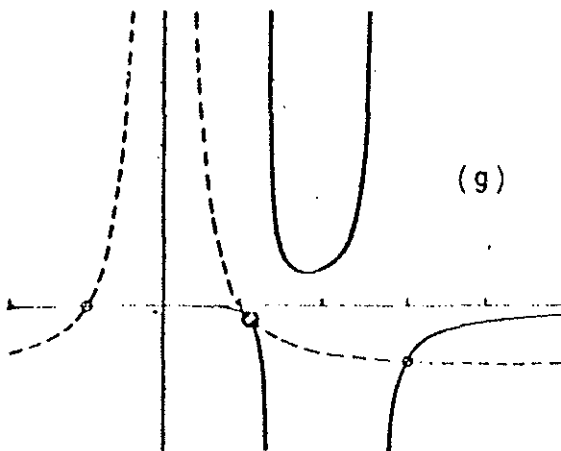
(d)



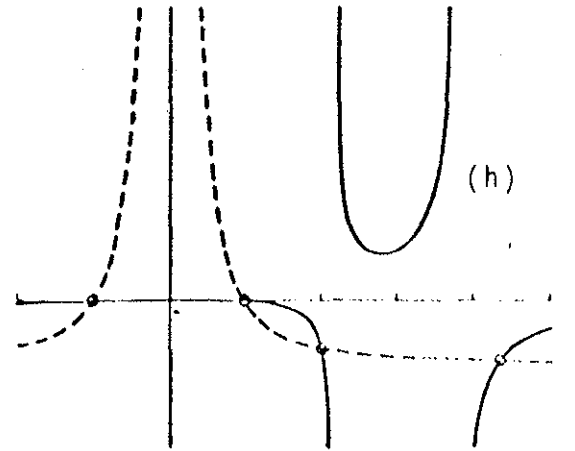
(e)



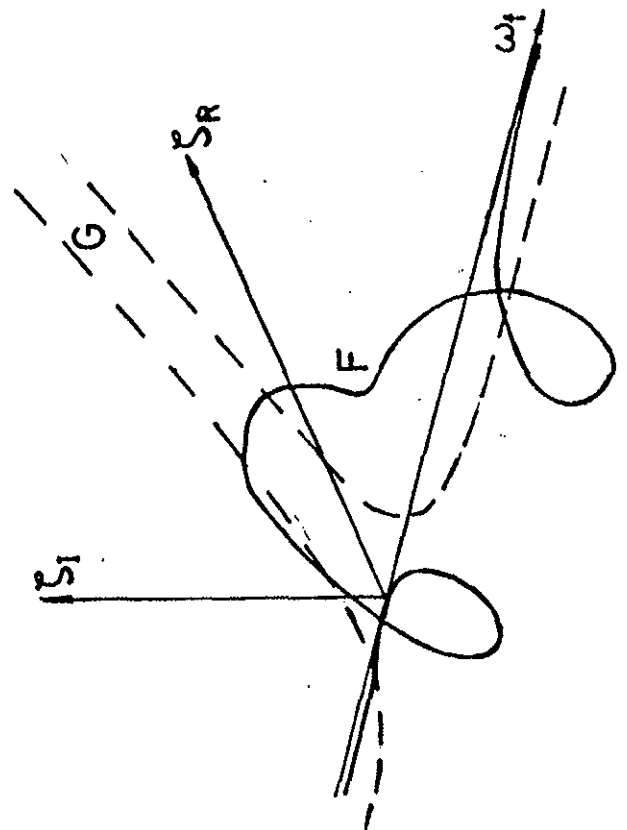
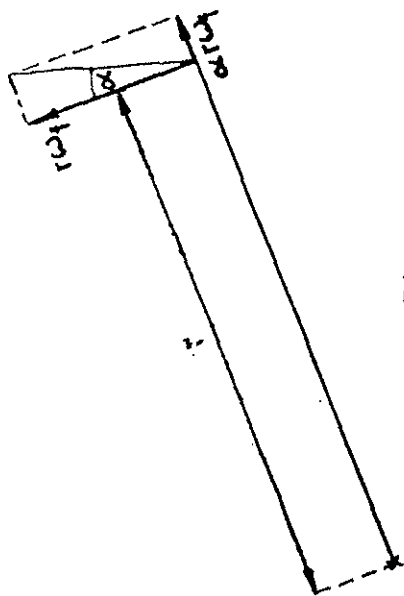
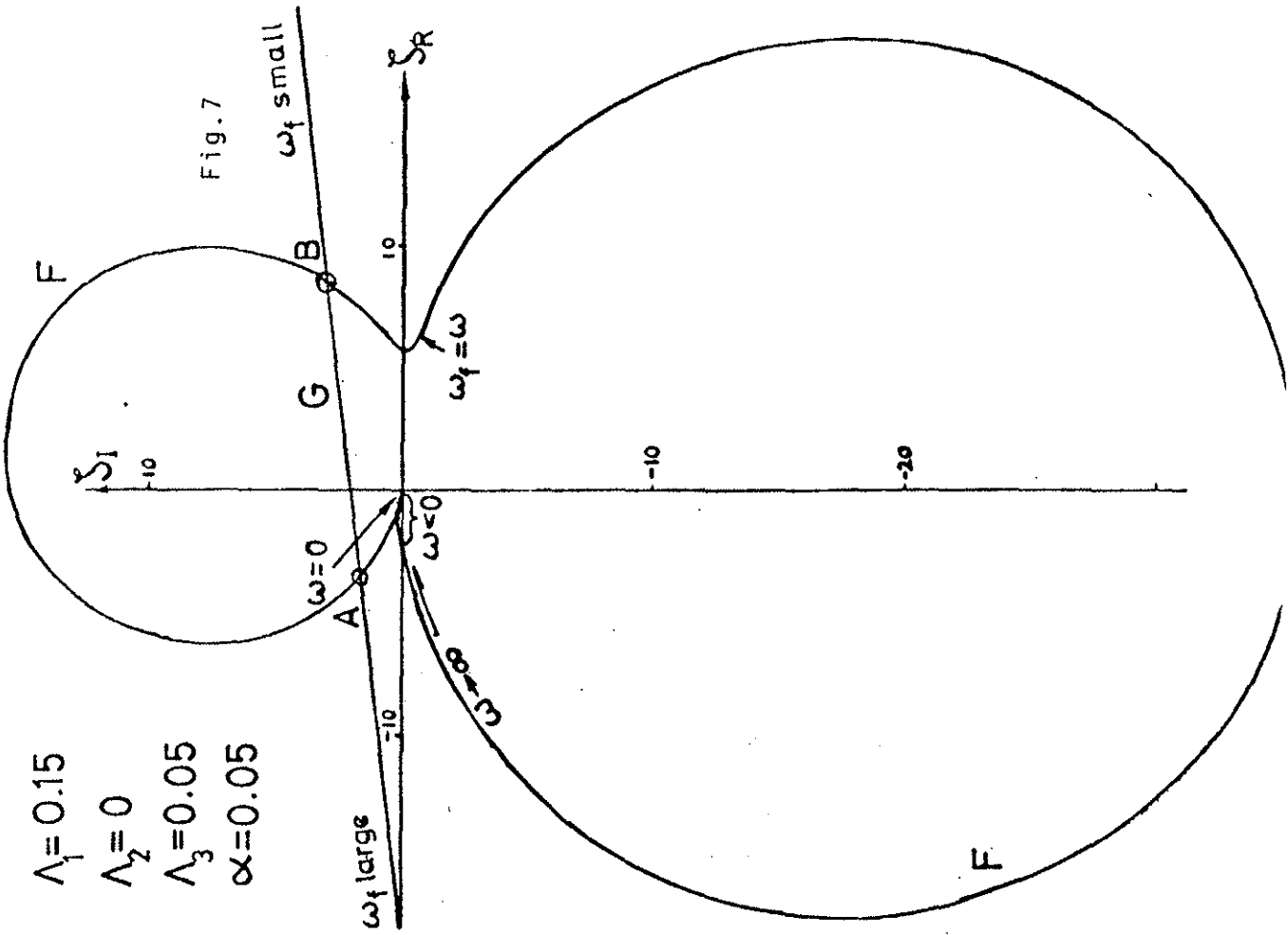
(f)



(g)



(h)



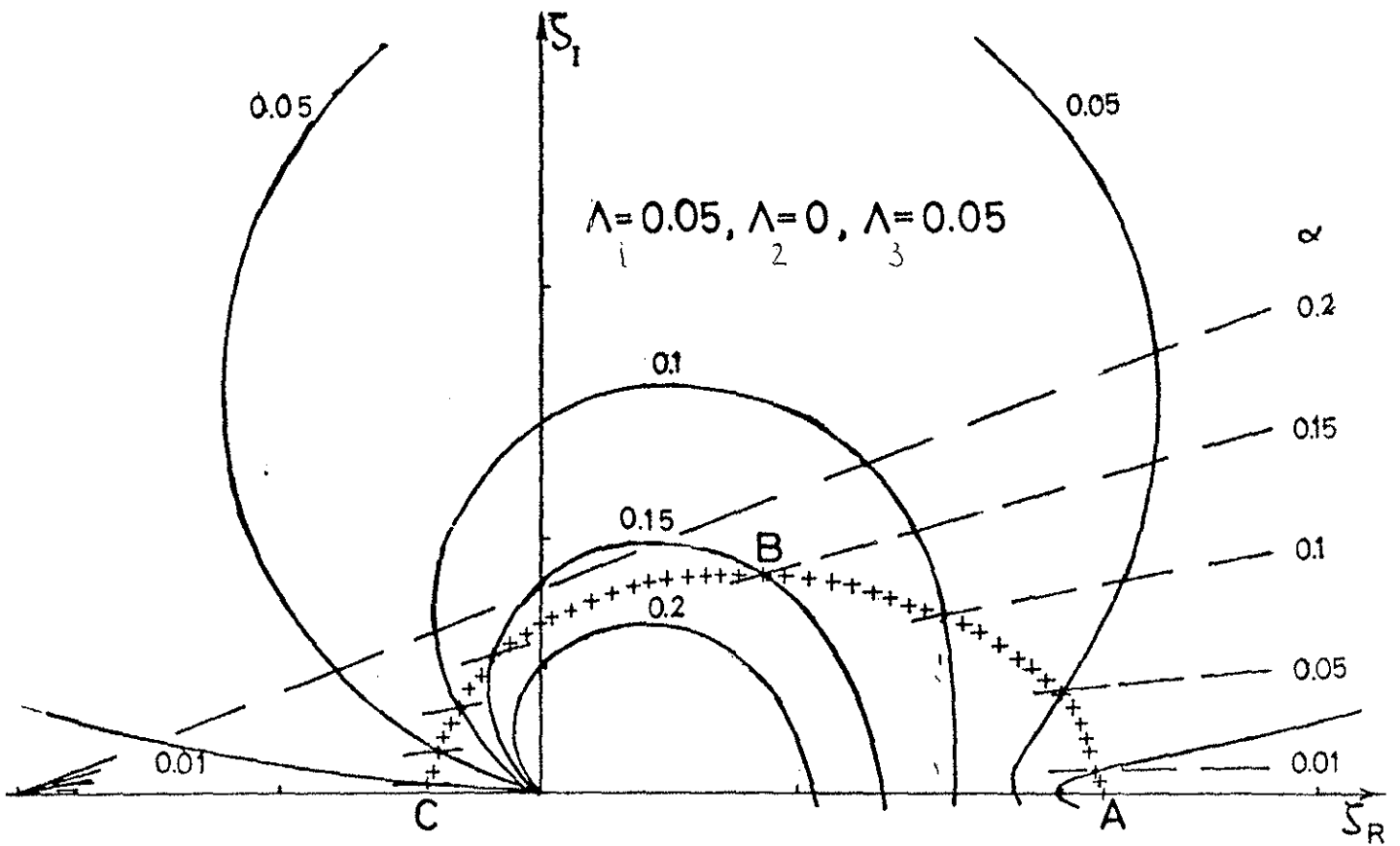


Fig. 8

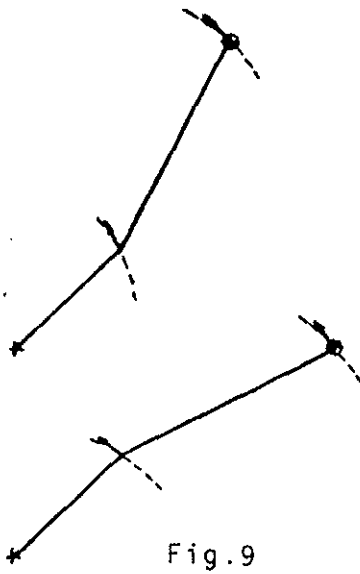


Fig. 9

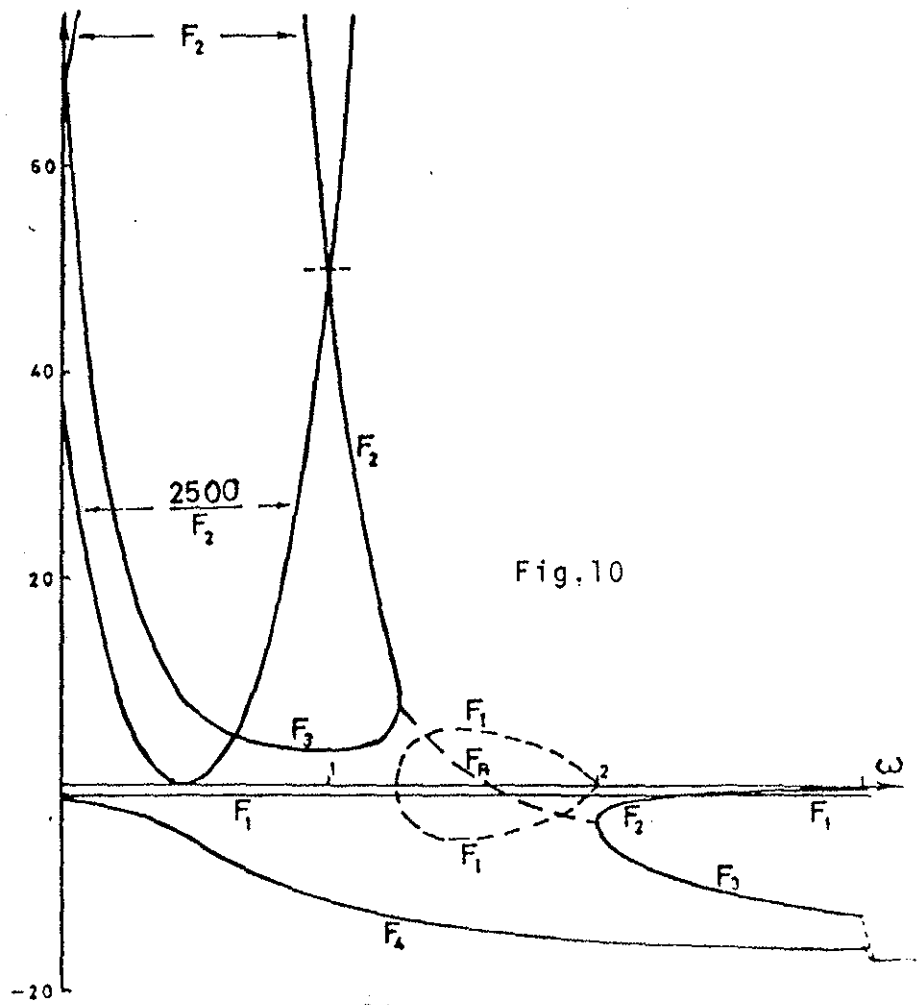
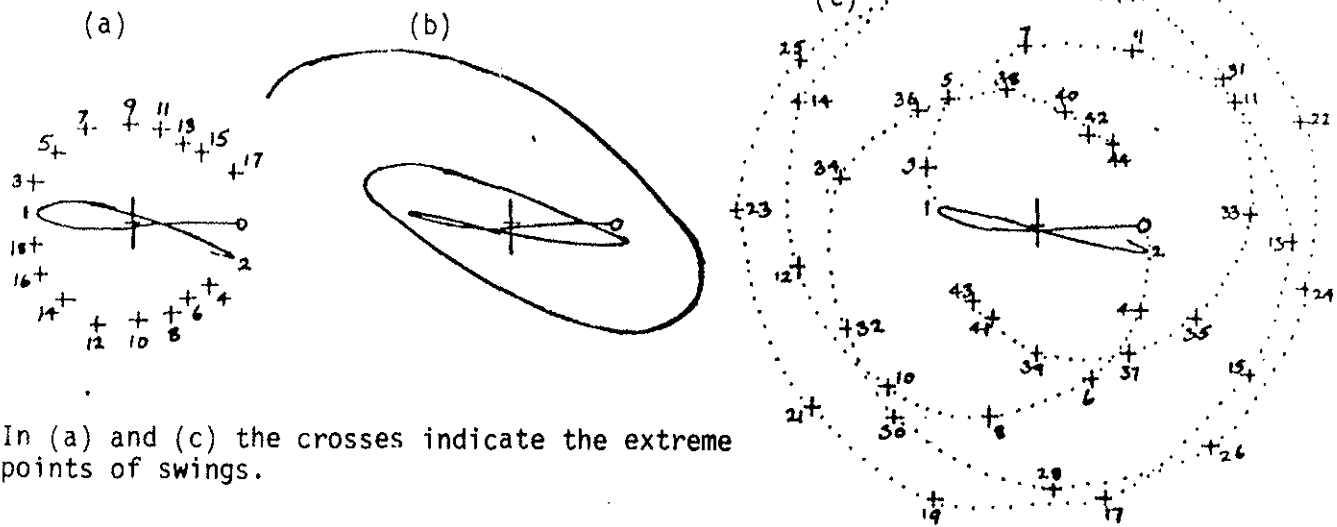


Fig. 10

Figure 11



In (a) and (c) the crosses indicate the extreme points of swings.

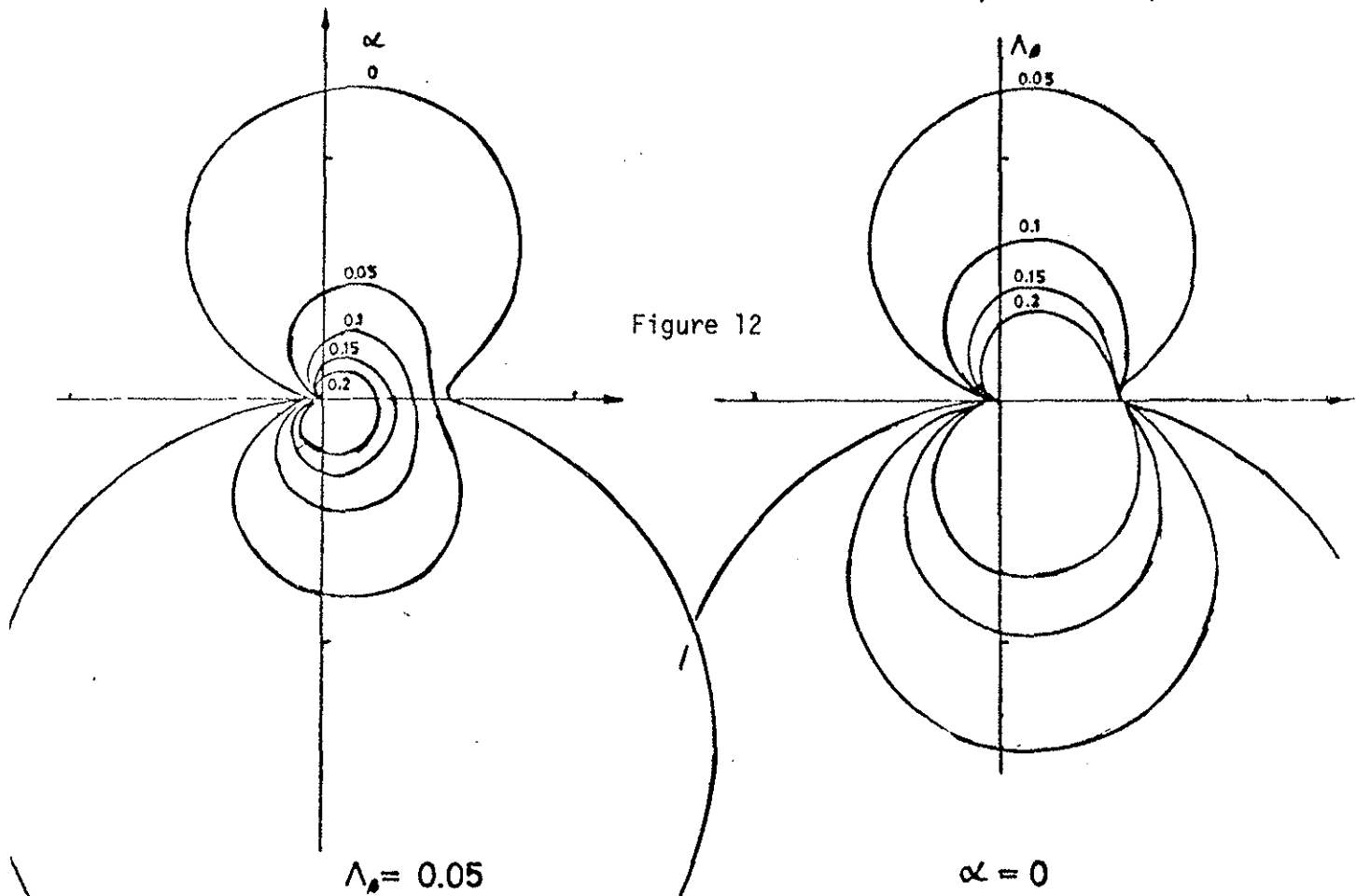
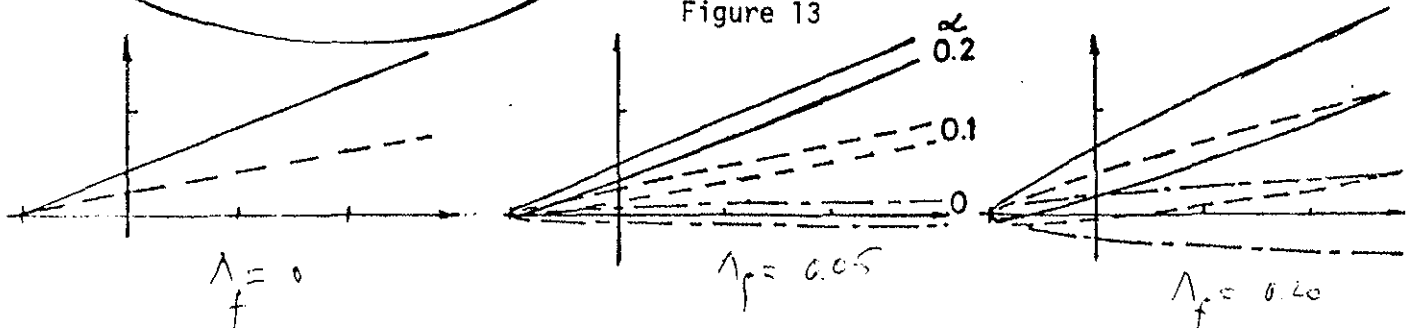


Figure 13



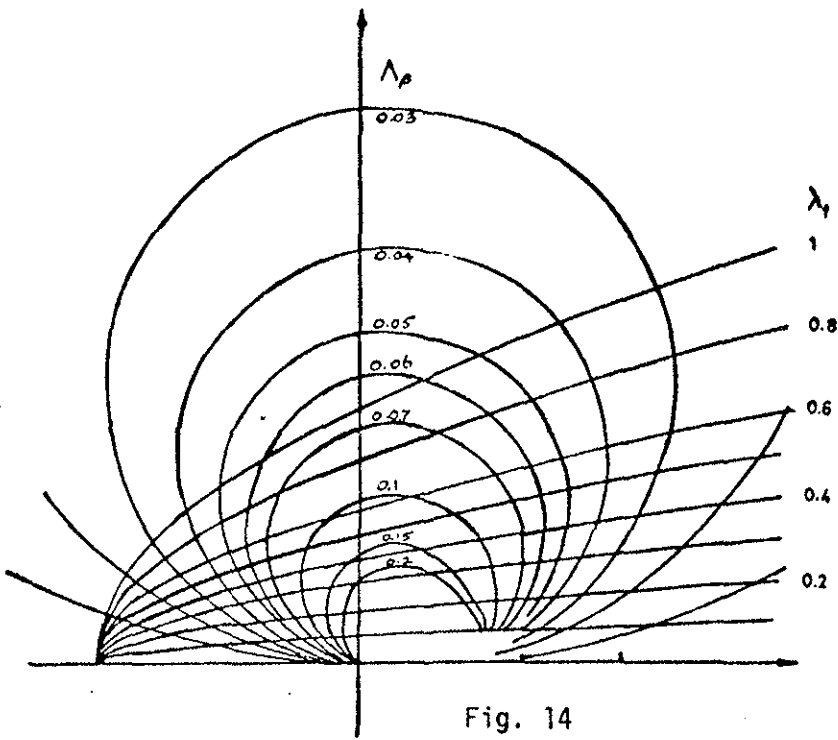


Fig. 14

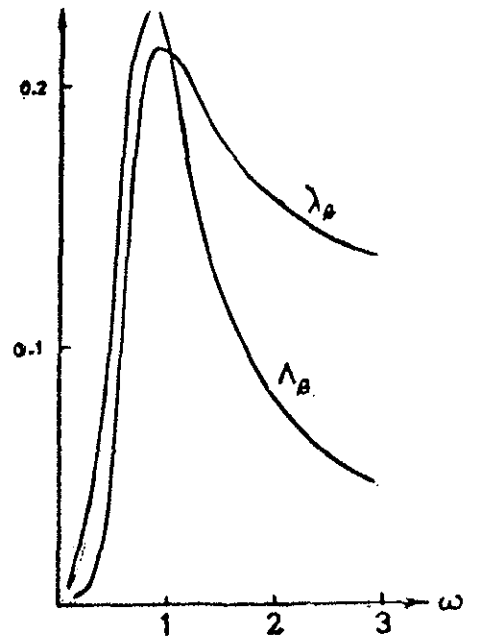


Fig. 15

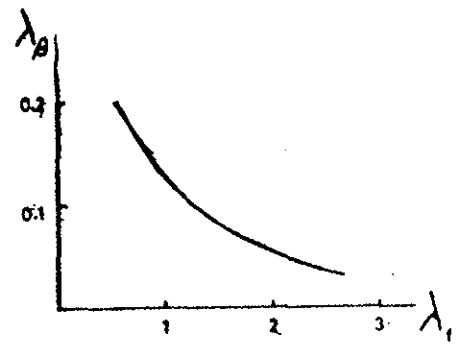


Fig. 16

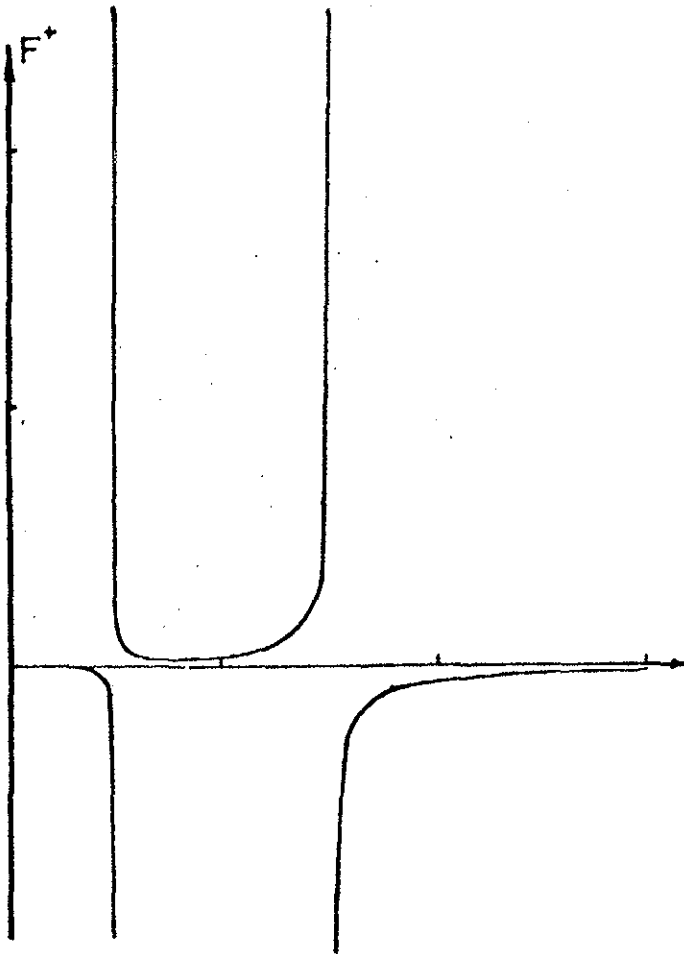


Fig. 17

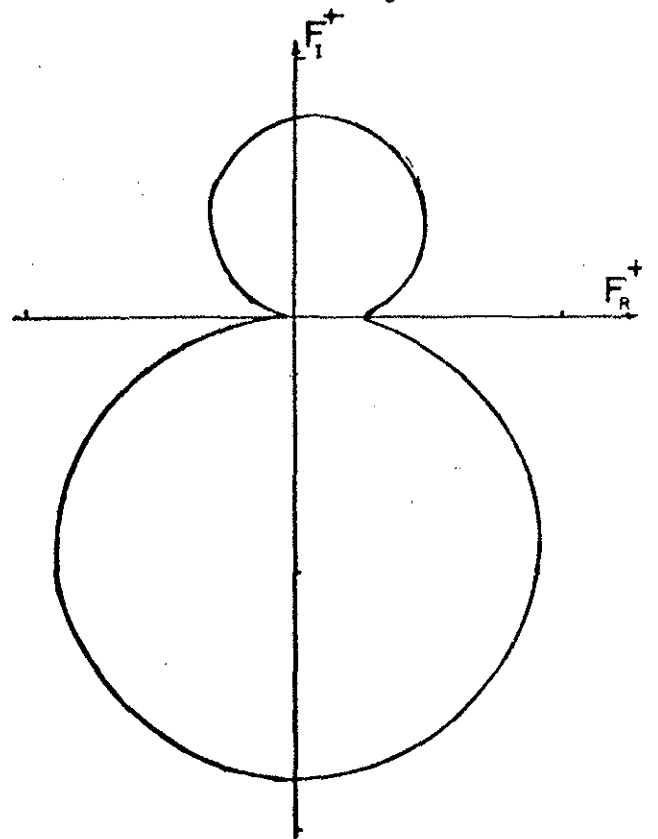


Fig. 18